The Single-crystal Electron Spin Resonance Spectrum of Oxobis(2-methylquinolin-8-olato)vanadium(IV) as a Pure Compound and Diluted in Chlorobis(2-methylquinolin-8-olato)gallium(III) †

David Collison, Brendan Gahan, and Frank E. Mabbs*
Chemistry Department, University of Manchester, Manchester M13 9PL

Single-crystal e.s.r. spectra of the compound $[VO(mquin)_2]$, diluted in $[GaCl(mquin)_2]$ (mquin = 2-methylquinolin-8-olate), at room temperature and *Q*-band frequencies are consistent with the retention of C_2 molecular symmetry in the diluted system. The spin-Hamiltonian parameters $g_{zz} = 1.949 \pm 0.002$, $g_{xx} = 1.988 \pm 0.002$, $g_{yy} = 1.983 \pm 0.002$, $A_{zz} = -(157.3 \pm 0.5) \times 10^{-4}$, $A_{xx} = -(50.8 \pm 0.5) \times 10^{-4}$, $A_{yy} = -(55.0 \pm 0.5) \times 10^{-4}$, and $A_{xy} = A_{yx} = (3.0 \pm 0.5) \times 10^{-4}$ cm^{-1} in conjunction with the electronic absorption spectra have been analysed *via* both angular overlap calculations and by constrained minimisation of a composite function of the expressions for the spin-Hamiltonian parameters to estimate the *d*-orbital mixing in the complex. A comparison of the results of these two approaches is made. The angular variation of the peak–peak linewidth of the first-derivative spectra in crystals of undiluted $[VO(mquin)_2]$ indicates an isotropic exchange between adjacent vanadium centres, in a three-dimensional arrangement, with $|J| = 380 \pm 20$ G.

In e.s.r. studies of undiluted single crystals of *d* transition-metal complexes information concerning the orientations of the molecular *g* tensor, as well as hyperfine coupling information, is often lost due to the influence of neighbouring paramagnetic centres.[1-6] The preferred way of overcoming the above difficulties is to dilute the paramagnetic compound in a diamagnetic isostructural host crystal. For oxovanadium(IV) compounds the ideal host would be the equivalent compound containing the MO^{2+} core, where M = Ti, Zr, Hf, Cr, Mo, or W. Unfortunately within this group of elements problems arise in that either monomeric compounds with terminal MO groups do not form readily or the relevant stable compounds have yet to be synthesised. As an alternative to this we are currently exploring the use of $GaCl^{2+}$ and $InCl^{2+}$ as equivalents for the VO^{2+} moiety. One such pair of structurally similar compounds is $[VO(mquin)_2]$ and $[GaCl(mquin)_2]$,[7] where mquin = 2-methylquinolin-8-olate, and we now report the results of a single-crystal e.s.r. study of $[VO(mquin)_2]$ as a pure material and diluted in $[GaCl(mquin)_2]$.

Experimental

Preparation of Compounds.—$[VO(mquin)_2]$ was prepared by the method of Shiro and Fernando.[7] Crystals suitable for e.s.r. measurements were grown from a toluene solution by concentration under reduced pressure.

The compound $[GaCl(mquin)_2]$ was prepared by mixing equimolar amounts of gallium metal dissolved in concentrated hydrochloric acid and 2-methylquinolin-8-ol in ethyl alcohol. The compound precipitated as a fine yellow powder. Crystals containing approximately 1% $[VO(mquin)_2]$, which were suitable for e.s.r. studies, were grown by the slow evaporation of an acetone solution. These crystals, and those of $[VO(mquin)_2]$ grown as above, had unit-cell parameters‡ the same as those reported previously.[7]

E.S.R. Spectra.—First-derivative spectra were obtained at room temperature on oriented (by standard *X*-ray techniques) single crystals of $[VO(mquin)_2]$ at both *X*- and *Q*-band frequencies, and on $[(GaCl,VO)(mquin)_2]$ at *Q*-band frequencies. The single crystals were oriented so that spectra could be obtained in the crystallographic a^*b, bc, and a^*c planes. Spectra on frozen toluene solutions of $[VO(mquin)_2]$ and on powdered $[(GaCl,VO)(mquin)_2]$ at both *X*- and *Q*-band frequencies were also obtained. The spectrometer used was a Varian E112, whilst cooling of the samples at *X*-band was achieved using an Oxford Instruments ESR9 continuous flow cryostat. The methods for obtaining the single-crystal spectra have been reported previously.[8]

Electronic Absorption Spectra.—These were obtained at room temperature between 1 500 and 300 nm using a Varian 2390 spectrometer.

Results and Discussion

Electronic Absorption Spectra.—The electronic absorption spectra of $[VO(mquin)_2]$ and $[GaCl(mquin)_2]$ in CH_2Cl_2, 1,2-$C_2H_4Cl_2$ solutions, and as poly(dimethylsiloxane) mulls are summarised in Table 1. Based on their molar absorption coefficients and the absence of similar features in the spectrum of $[GaCl(mquin)_2]$, the first three bands in the $[VO(mquin)_2]$ spectra are assigned to *d–d* transitions. The band at *ca.* 26 000 cm^{-1} of $[VO(mquin)_2]$ is assigned as a charge-transfer band based on its relatively high absorption coefficient, the sensitivity of the latter to solvent, and on the presence of a band at a similar frequency for $[GaCl(mquin)_2]$. This assignment compares favourably with that deduced by Collison *et al.*[9] from single-crystal and mull studies on five-co-ordinate complexes of approximately square-pyramidal geometry where all the *d–d* bands occurred below 26 000 cm^{-1}, and those given by Selbin and Morpurgo[10] on low-symmetry oxovanadium(IV) complexes. Studies[11] on the structurally similar, but less distorted trigonal-bipyramidal molecule $[VOCl_2(NMe_3)_2]$ (C_{2v}) revealed four weak bands at 11 760 (ε = 45), 13 150 (76), 14 200 (12), and 27 030 cm^{-1} (12 dm^3 mol^{-1} cm^{-1}) which were assigned to *d–d* transitions. The small absorption coefficients for all of these *d–d* bands lend support for our proposed assignment

† *Non-S.I. unit employed:* G = 10^{-4} T.

‡ $[VO(mquin)_2]$: space group $C2/c$, a = 17.045, b = 7.843, c = 13.400 Å, β = 105°14′, Z = 4. $[GaCl(mquin)_2]$: space group $C2/c$, a = 28.884, b = 9.594, c = 15.199 Å, β = 118°43′, Z = 8.

Table 1. Electronic absorption spectra of $[VO(mquin)_2]$ and $[GaCl(mquin)_2]$

Compound	Medium	Wavenumber of band maximum ($\times 10^{-3}$ cm^{-1})	Molar absorption coefficient, ε/dm^3 mol^{-1} cm^{-1}
$[VO(mquin)_2]$	CH_2Cl_2	13.42	25
		17.24	32
		20.00(sh)	*ca.* 49
		26.32	706
	$1,2\text{-}C_2H_4Cl_2$	13.42	18
		17.24	19
		20.00(sh)	*ca.* 30
		25.97	4 822
	Poly(dimethylsiloxane) mull	13.70, 17.24, 20.00, 25.00	all v br
$[GaCl(mquin)_2]$	CH_2Cl_2	27.40	2 194
	$1,2\text{-}C_2H_4Cl_2$	27.17	4 444
	Poly(dimethylsiloxane) mull	24.69, 26.32, 37.04(sh), 38.76	all br

sh = Shoulder, br = broad.

Table 2. Principal values of the g^2 and A^2 tensors and their direction cosines with respect to the crystal axes

	Alternative 1			Alternative 2			
g^2	a^*	b	c	g^2	a^*	b	c
g^2_{11} 3.799	−0.1099	−0.3325	0.9367	g^2_{11} 3.799	−0.1282	0.3369	0.9328
g^2_{22} 3.934	0.7603	−0.6352	−0.1363	g^2_{22} 3.942	0.8655	0.4973	−0.0607
g^2_{33} 3.954	−0.6403	−0.6972	−0.3225	g^2_{33} 3.947	0.4843	−0.7995	0.3553
$A^2/10^{-4}$ cm^{-1}				$A^2/10^{-4}$ cm^{-1}			
A^2_{11} 2.473	−0.1087	−0.3332	0.9366	A^2_{11} 2.466	−0.0933	0.3299	0.9394
A^2_{22} 0.2420	0.9189	0.3258	0.2225	A^2_{22} 0.1554	0.7674	−0.5773	0.2789
A^2_{33} 0.3207	0.3793	−0.8848	−0.2707	A^2_{33} 0.4143	0.6344	0.7469	−0.1993

Direction cosines between the principal g^2 and A^2 tensors

	Alternative 1				Alternative 2		
	A^2_{11}	A^2_{33}	A^2_{22}		A^2_{11}	A^2_{33}	A^2_{22}
g^2_{11}	1.0000	−0.0011	−0.0008	g^2_{11}	0.9993	−0.0156	−0.0327
g^2_{22}	0.0014	0.8872	0.4613	g^2_{22}	0.0263	0.9325	0.3601
g^2_{33}	−0.0002	0.4613	−0.8872	g^2_{33}	0.0249	−0.3608	0.9323

of the spectrum of $[VO(mquin)_2]$ despite the similarity in frequency of the fourth band in the spectra of each of these compounds.

E.S.R. Spectra.—The first-derivative e.s.r. spectra of single crystals of $[VO(mquin)_2]$ at both *X*- and *Q*-band frequencies showed a single broad line, with no vanadium hyperfine structure, at all orientations in the a^*b, bc, and a^*c crystallographic planes. However the peak–peak linewidth, ΔB_{P-P}, and the *g* values varied with orientation as shown in Figure 3. Simulation* of the spectra showed them to be essentially Gaussian but with an approximate 25% Lorentzian contribution depending upon the orientation. Since each $[VO(mquin)_2]$ molecule in the unit cell has the V=O vector parallel to the *b* axis which is also an axis of C_2 symmetry, we can assign the *g* value parallel to *b* and the maximum and minimum values in the a^*c plane to the principal molecular *g* values, *i.e.* $g_{zz} = 1.947$, $g_{xx} = 1.987$, and $g_{yy} = 1.981$. The estimated error on each of these *g* values is ± 0.002.

The first-derivative e.s.r. spectra of single crystals of $[(GaCl,VO)(mquin)_2]$ at *Q*-band frequencies showed well resolved vanadium hyperfine splittings at all orientations of the crystals in the magnetic field. As expected for these monoclinic crystals, overlapping eight-line spectra from each magnetically inequivalent molecule in the a^*b and bc planes were observed. However, in the a^*c plane a single eight-line spectrum was observed since the molecules are magnetically equivalent in this plane. The data from these spectra were analysed by the methods of Schonland[12] and Lund and Vanngard[13] to give the principal values and directions of the *g* and *A* tensors, see Table 2.

* Simulations of the line shape for the undiluted compound *only* were performed using the SIMU routine of the Varian E-900 data acquisition system. Input parameters were the effective *g* value, the peak–peak linewidth, and the percentage Lorentzian contribution.

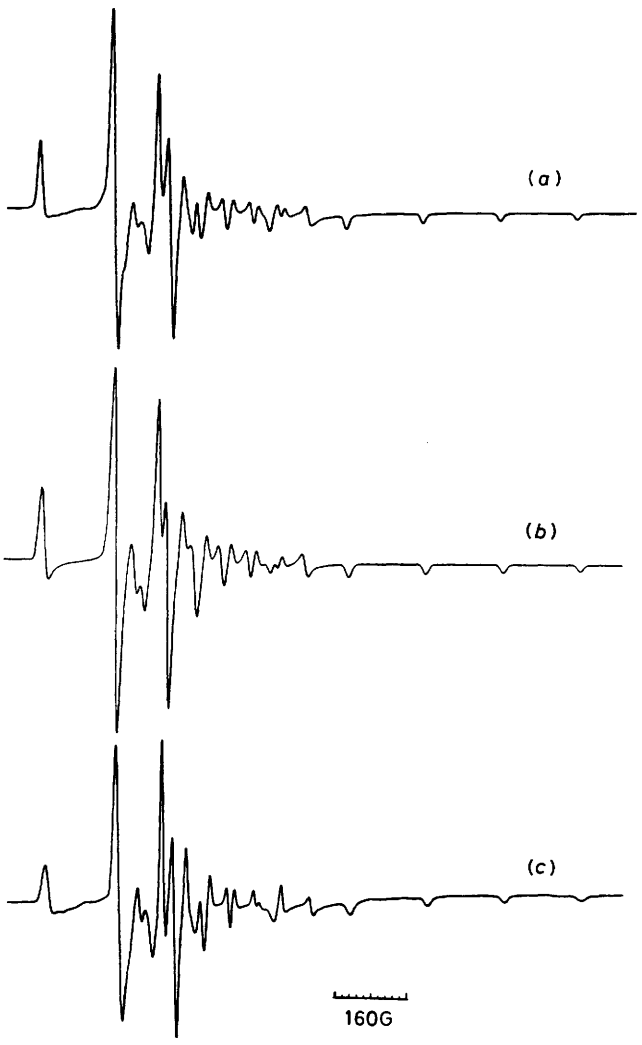

Figure 1. E.s.r. spectra at *Q*-band (34.994 GHz), each starting at 12 000 G. (*a*) Frozen saturated toluene solution of $[VO(mquin)_2]$ at 150 K; (*b*) powdered $[(GaCl,\{1\%\ VO\})(mquin)_2]$ at 300 K; (*c*) simulation using alternative 1 in Table 2, molecular peak–peak linewidths referred to the *g* tensor axes of $\Delta B_{xx} = 11.0$, $\Delta B_{yy} = 11.3$, $\Delta B_{zz} = 13.0$ G, and a Gaussian line-shape function

The e.s.r. spectra of powdered $[(GaCl,VO)(mquin)_2]$ and of a frozen toluene solution of $[VO(mquin)_2]$ are identical to each other at both *X*- and *Q*-band frequencies, see Figures 1 and 2. These observations are consistent with the same geometry for $[VO(mquin)_2]$ in both media. Simulation of these spectra based on methods described previously[14,15] has enabled us to distinguish between the two alternatives in Table 2. Alternative 1 which produces the closest simulations is preferred and will be used in the subsequent discussions.

The single-crystal e.s.r. spectra of $[(GaCl,VO)(mquin)_2]$ are consistent with $[VO(mquin)_2]$ occupying the molecularly more distorted $[GaCl(mquin)_2]$ sites in the crystal. Also the coincidence of g_{11} and A_{11}, plus the identical nature of the powdered $[(GaCl,VO)(mquin)_2]$ and frozen-solution spectra of $[VO(mquin)_2]$, indicate that the $[VO(mquin)_2]$ molecule retains its C_2 symmetry in the diluted crystal. The principal *g* values, see Table 2 ($g_{11} = 1.949$, $g_{22} = 1.988$, $g_{33} = 1.983$), are within experimental error of the principal values found in the undiluted crystal. We therefore assume that g_{11} in the diluted crystal is parallel to V=O. However, g_{11} is not parallel to the

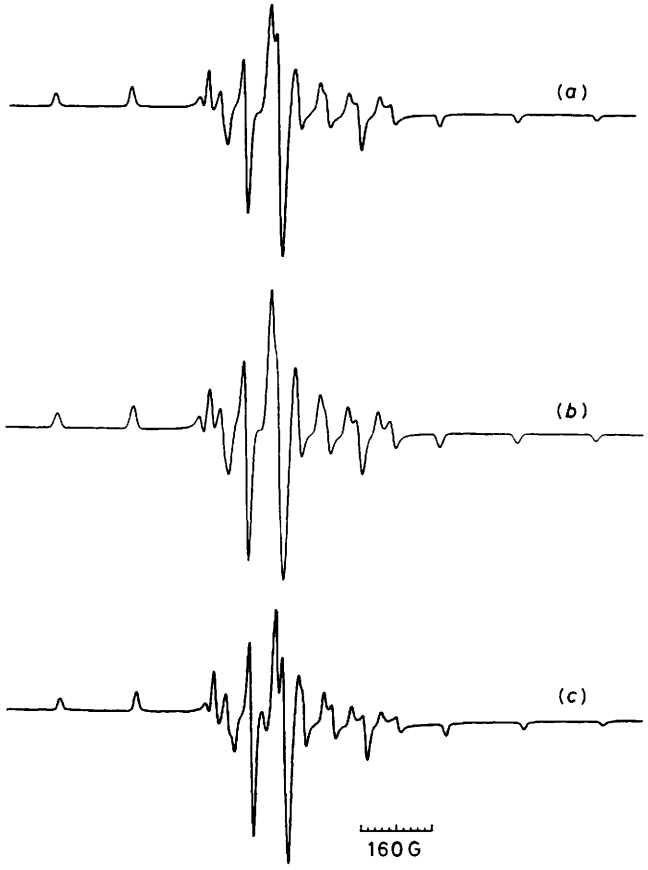

Figure 2. E.s.r. spectra at *X*-band (9.250 GHz), each starting at 2 500 G. (*a*) Frozen saturated toluene solution of $[VO(mquin)_2]$ at 77 K; (*b*) powdered $[(GaCl,\{1\%\ VO\})(mquin)_2]$ at 300 K; (*c*) simulation using the conditions in Figure 1(*c*)

Ga–Cl vector, the angle between them being 11.7°. This indicates that, although the vanadium compound has substituted into the specific crystallographic sites, the metal–ligand bonds of the vanadium and gallium compounds do not coincide in the crystal. Thus, although the e.s.r. spectra of the diluted system give the relationship between the *g* and *A* tensors, they do not completely define their relationship to the molecular geometry of the $[VO(mquin)_2]$ molecule. Two of the principal axes of each tensor lie in a plane perpendicular to the terminal V=O vector, as they must for C_2 symmetry. However, there is no requirement in this symmetry for these two axes of each tensor to coincide, and we observe that A_{22} and A_{33} are rotated by 27.5° from g_{33} and g_{22}, respectively. The principal values of the *A* tensor are $A_{11} = -157.3 \times 10^{-4}$, $A_{22} = -49.2 \times 10^{-4}$, and $A_{33} = -56.6 \times 10^{-4}$ cm^{-1}.

Relationship between the Electronic Structure, E.S.R. Parameters, and Electronic Absorption Spectrum of $[VO(mquin)_2]$.—In the point group C_2, with the two-fold axis parallel to V=O, the allowed *d*-orbital mixings are as in equations (1)—(5) where

$$\psi_1 = \alpha(a_1 d_{x^2-y^2} + b_1 d_{xy} + c_1 d_{z^2}) \quad (1)$$

$$\psi_2 = \beta(a_2 d_{x^2-y^2} + b_2 d_{xy} + c_2 d_{z^2}) \quad (2)$$

$$\psi_3 = \gamma(e_3 d_{xz} + f_3 d_{yz}) \quad (3)$$

$$\psi_4 = \delta(e_4 d_{xz} + f_4 d_{yz}) \quad (4)$$

$$\psi_5 = \varepsilon(a_5 d_{x^2-y^2} + b_5 d_{xy} + c_5 d_{z^2}) \quad (5)$$

Table 3. Ranges of angular overlap parameters (10^3 cm^{-1})

Donor atom	e_σ	e_{π_x}	e_{π_y}
Terminal oxygen	16—17	12—13	12—13
mquin oxygen	6—7	0—0.8	0—0.6
mquin nitrogen	6—7	0—0.8	Constrained to be zero

within fairly narrow ranges. These ranges for the various donor-atom types are summarised in Table 3. The signs and magnitudes of the parameters[18] are consistent with the expected strong σ- and π-donor properties of the terminal oxo group and good σ-donor but poor π-donor or -acceptor abilities of the oxygen and nitrogen atoms in the mquin ligands. With the exception of e_{π_x} for the quinolinato nitrogen atom, the relative magnitudes and signs of the e_σ parameters and the e_π

Table 4. An example of the parameters from an angular overlap calculation required to reproduce the experimental data

			$e/10^4$ cm^{-1}		
Ligand	θ/°	φ/°	σ	π_x	π_y
Terminal oxo	0.0	0.0	1.60	1.20	1.20
mquin oxygen	116.4	336.0	0.6	0.06	0.02
	116.4	156.0	0.6	0.06	0.02
mquin nitrogen	99.5	251.9	0.6	0.06	0.00
	99.5	71.9	0.6	0.06	0.00

		d-Orbital mixing coefficients				
Relative energy/10^3 cm^{-1}	Orbital	a_i	b_i	c_i	e_i	f_i
0	ψ_1	0.6591	0.7513	−0.0338	—	—
12.867	ψ_2	−0.6862	0.6192	0.3813	—	—
12.940	ψ_3	—	—	—	−0.4367	−0.8996
17.733	ψ_4	—	—	—	−0.8996	0.4367
20.305	ψ_5	−0.3078	0.2285	−0.9236	—	—

These *d*-orbital mixing coefficients plus the following parameters $\alpha^2 = 0.95 \pm 0.05$, $\beta^2 = 0.59 \pm 0.01$, $\varepsilon^2 = 0.55 \pm 0.05$, $\gamma^2 = 0.86 \pm 0.06$, $\delta^2 = 0.83 \pm 0.04$, $P = (122 \mp 6) \times 10^{-4}$ cm^{-1}, and $\xi_V = 160 \mp 10$ cm^{-1} give calculated spin-Hamiltonian parameters $g_{zz} = 1.949 \pm 0.001$, $g_{xx} = 1.988 \pm 0.001$, $g_{yy} = 1.983 \pm 0.001$, $A_{zz} = -(157.1 \pm 0.1) \times 10^{-4}$, $A_{xx} = -(49.7 \pm 0.01) \times 10^{-4}$, $A_{yy} = -(55.4 \pm 0.1) \times 10^{-4}$, and $A_{xy} = A_{yx} = 3.0 \times 10^{-4}$ cm^{-1}.

α, β, γ, δ, and ε are the metal coefficients in the antibonding molecular orbitals. The *g* and *A* tensor elements can be computed from these equations by using the perturbation expressions of Abragam and Bleaney.[16] The resulting equations show a complicated non-linear dependence on the *d*-orbital coefficients (see Appendix) and it is possible to obtain a first-order estimate of the mixing coefficients in the ground state only, by working in the diagonalised *g*-axis framework. The *d*-orbital mixing in the excited states which makes a significant contribution to the *g* tensor cannot be calculated in this way. In order to overcome this difficulty we have used two approaches. First we have employed an angular overlap model, as described by Gerloch and Slade,[17] to calculate the energies of and the mixing coefficients in the metal *d* orbitals. The principal axes of the *g* tensor were chosen to be the molecular axes, *i.e.* *z* is along the terminal V=O ($g_{11} = g_{zz} = 1.949$), *x* is coincident with $g_{22}(= g_{xx} = 1.988)$, and *y* is coincident with $g_{33}(= g_{yy} = 1.983)$. The input to the model involves the angular overlap parameters, e_σ, e_{π_x}, e_{π_y} and the polar angles θ and φ for each ligand. The angles θ and φ were calculated from the crystallographic information[7] and the orientation of g_{22} and g_{33} obtained from the e.s.r. spectra of crystals of undiluted [VO(mquin)$_2$].

The calculation proceeded by varying the angular overlap parameters (with the exception of e_{π_x} for the quinolinato nitrogen atom which was constrained to be zero[18]) until all the *d*–*d* transitions were calculated to be within ± 1 000 cm^{-1} of the peak maxima which we have attributed to *d*–*d* transitions in the electronic absorption spectrum (see above).

There is no unique set of angular overlap parameters which will reproduce the electronic absorption spectrum. However the constraint of the four possible *d*–*d* transitions being between *ca.* 13×10^3 and 20×10^3 cm^{-1} with two of them being almost coincident does lead to the angular overlap parameters falling

parameters for the phenolic oxygen and quinolinato nitrogen are in accord with the same relationships of these parameters in a number of nickel(II) and cobalt(II) complexes.[18–21] In the present d^1 system where the π orbital of the quinolinato nitrogen atom interacts with formally empty metal *d* orbitals, we find weak π-donor behaviour in contrast to the π-acceptor behaviour of this donor atom in the d^7 and d^8 cobalt(II) and nickel(II) complexes.

The eigenfunctions from the angular overlap calculation plus the observed *g* and *A* tensor elements expressed in the *g* tensor axis system* were used to obtain values for $P(= 2g_N\beta_N\beta_e\langle r^{-3}\rangle)$ and the molecular-orbital coefficients *via* the equations in the Appendix. In this treatment we have taken values of ξ_V[22] for a formal oxidation state corresponding to that indicated by the calculated value of *P*,[23] see equation (6) where ξ_V is in cm^{-1} and

$$\xi_V = 1.8182P - 62.73 \quad (6)$$

P in units of 10^{-4} cm^{-1}. During the course of these calculations we found that it was not possible simultaneously to obtain a diagonal *g* tensor and the correct sign of A_{xy} using the ligand φ values calculated as described above. It was necessary to allow the *g* tensor axes to rotate with respect to the molecular framework. However the changes in φ required were small, $< 6°$ from those calculated directly from the crystallographic information as described above. An example of a set of parameters which gives a good reproduction of the experimental data is in Table 4. Because there is a significant correlation between *P*, ξ_V, and some of the *d*-orbital molecular-orbital parameters in equations (A1)—(A9), a unique set of

* The *A* tensor elements in the *g* tensor axis framework are $A_{zz} = -157.3 \times 10^{-4}$, $A_{xx} = -50.8 \times 10^{-4}$, $A_{yy} = -55.0 \times 10^{-4}$, and $A_{xy} = A_{yx} = 3.0 \times 10^{-4}$ cm^{-1}.

Table 5. An example of the parameters required to reproduce the experimental e.s.r. data using the method of constrained minimisation *

Relative energy/10^3 cm^{-1}	Orbital	*d*-Orbital mixing coefficients a_i	b_i	c_i	e_i	f_i	Molecular-orbital coefficient
0	ψ_1	0.489	0.845	−0.030	—	—	1.000
13.420	ψ_2	−0.732	0.454	0.517	—	—	0.854
13.420	ψ_3	—	—	—	0.870	−0.492	0.854
17.240	ψ_4	—	—	—	−0.492	−0.870	1.000
20.000	ψ_5	0.463	−0.244	0.854	—	—	0.700

	xx	*yy*	*zz*	*xy*	*yx*
A_{ij} obs.†	−50.8	−55.0	−157.3	3.0	3.0
A_{ij} calc.†	−50.8	−55.0	−157.3	3.0	3.0
g_{ij} obs.	1.988	1.983	1.949	0.0	0.0
g_{ij} calc.	1.988	1.985	1.949	0.0	0.0

* Obtained using minimisation of F with all $w_k = 1.0$, $\rho A_{ii} = 0.01$, $\rho A_{ij} = 0.05$, and $\rho g_{ij} = 0.001$. $P = 116.1 \times 10^{-4}$ cm^{-1} and $\xi_V = 148.4$ cm^{-1}. † In units of 10^{-4} cm^{-1}.

these parameters cannot be determined. The values of P and ξ_M depend upon the charge on the metal atom in the complex[22,23] and a suitable choice of these parameters has always presented a problem.[15,24-26] However, with the assumption that we would expect $1.0 \geqslant \alpha^2 > \gamma^2$, $\delta^2 \geqslant \beta^2 \geqslant \varepsilon^2 \geqslant 0.5$ the range of acceptable parameters is greatly reduced. Thus for the angular overlap parameters in Table 4 we find α^2 is between 0.90 and 1.00 and P between 126×10^{-4} and 114×10^{-4} cm^{-1}. These values of P correspond to formal charges on the vanadium atom in the complex of +2.0 and +1.5, respectively.[23]

The second method of determining *d*-orbital mixing coefficients (m_i) and metal molecular-orbital coefficients (χ_j) in low-symmetry molecules for the general eigenfunction $\psi_j = \chi_j \sum_i m_i \varphi_i$ is to use both the observed electronic absorption and e.s.r. spectra in a symmetry-determined empirical method. We outline here such a method based on the NAG algorithm E04UAF[27] designed to minimise a function with continuous first and second derivatives.[28,29] The variables are subject to fixed bounds with provisions for equality, inequality, and range constraints. Solutions to equations (1)—(5) are required such that values of m_i, χ_i, and P (see above) form a self-consistent set of values which calculate *all* the e.s.r. spin-Hamiltonian parameters of equations (A1)—(A9) within the limits of experimental observation.

The minimisation was subjected to the following constraints. (*a*) Equalities: (1) $g_{xy} = g_{yx} = 0$; (2) $A_{xy} = A_{yx}$; (3)—(12) normalisation of *d* functions [see equations (A10) and (A11)]; (13)—(16) orthogonalisation of the *d* functions [see equation (A12)]; and (17)—(18) the sense of the anisotropy, *i.e.* $A_{xx} - A_{yy} = +4.2 \times 10^{-4}$ cm^{-1} and $g_{xx} - g_{yy} = +0.005$. (*b*) Inequalities: (1) the highest-energy *d*–*d* transition, Δ_5, is assigned to be a one-electron promotion into an orbital which is predominantly $3d_{z^2}$ in character, *i.e.* $c_5^2 \geqslant 0.55$; (2)—(6) the *d*-orbital molecular-orbital coefficients are assumed to obey $1.0 \geqslant \alpha^2 > \gamma^2$, $\delta^2 \geqslant \beta^2 \geqslant \varepsilon^2 \geqslant 0.5$. (*c*) Ranges: The spin-Hamiltonian parameters (O) were calculated using equations (A1)—(A9). The differences, $(O_{calc.} - O_{obs.})$, were subjected to user-defined ranges based on the quality of the experimental data. The solutions to the problem are bounded such that: (*i*) $-1.0 \leqslant m_i \leqslant +1.0$; (*ii*) $0.5 \leqslant \chi_j^2 \leqslant 1.0$; and (*iii*) $100.0 \leqslant P \leqslant 180.0$ in units of 10^{-4} cm^{-1}.

The suitability of various functions to be minimised was assessed and a weighted composite function, F [equation (7)], of all the e.s.r. observables was found to be most appropriate where

$$F = \sqrt{F'/n} \qquad (7)$$

n = number of independent e.s.r. parameters [*e.g.* equations (A1)—(A9)] and F' is given by equation (8) for all $i,j = x,y,z$. w_k and w_l are weighting factors, $\delta O_{ij} = (O_{ij(calc.)} - O_{ij(obs.)})$ and ρO_{ij} is a user-acceptable tolerance between $O_{ij(calc.)}$ and $O_{ij(obs.)}$. The function F' was constructed in this way so that g_{ij} and A_{ij} are similar numerically and because the minimisation procedure is most efficient when all constraints and unknowns are in the range −1 to +1. Values of Δ_i are taken from Table 1 and the relationship between P and ξ_V from equation (6).

$$F' = \sum_{i,j} w_k(\delta A_{ij}/\rho A_{ij})^2 + \sum_{i,j} w_l(\delta g_{ij}/\rho g_{ij})^2 \qquad (8)$$

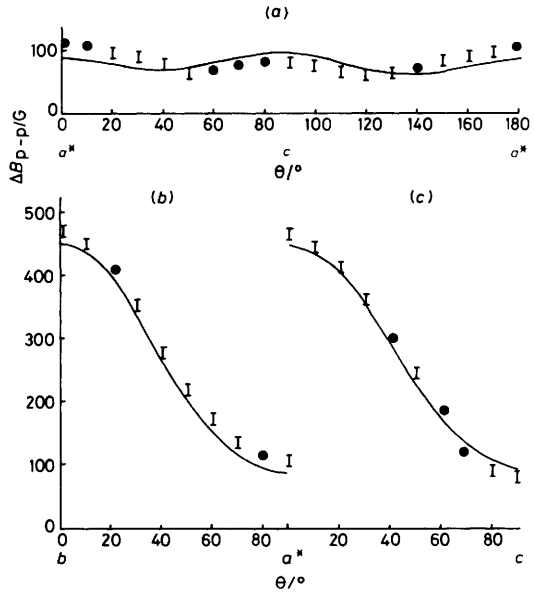

Figure 3. Comparison of the observed (I) and calculated ($|J| = 380$ G) (———) linewidths in the crystallographic planes (*a*) *a***c*, (*b*) *ba**, and (*c*) *bc*. The error bars represent the spread of peak–peak linewidths measured at the two different frequencies

The results of this calculation are in Table 5 and show a similar pattern of *d*-orbital mixing to that given by the angular overlap calculation. The most serious discrepancy is the reversal of the composition of ψ_3 and ψ_4 compared to the angular overlap model. However we believe that this comparison demonstrates that the constrained minimisation method can yield a valuable first approximation to the *d*-orbital mixing particularly in the ground state, and also to the other parameters. Such an approach will be of value for interpreting

the spin-Hamiltonian parameters of low-symmetry systems for which detailed structural information is lacking but where the symmetry can be inferred from the e.s.r. spectra and chemically sensible arrangements of the ligands.

The angular variation of the peak–peak linewidth for pure $[VO(mquin)_2]$ has been analysed *via* equation (9), which is based on the assumption of a three-dimensional isotropic exchange interaction and a Gaussian line-shape function,[30]

$$\Delta B_{p-p} \simeq M_2^T/|J| \quad (9)$$

where $M_2^T = M_2^d + M_2^h$ is the total second moment,[31] M_2^d = the second moment arising from dipolar interactions between neighbouring magnetic dipoles in the lattice,[30] M_2^h = the contribution to the second moment from the hyperfine interaction, and J = isotropic exchange parameter. Values of M_2^h were calculated from the resonance positions obtainable from our simulation program, using an adaptation of the general treatment of second moments given by Slichter.[32] This allows us readily to include the effects of the non-coincidence of the g and A tensors and also second-order effects. A comparison of the observed and calculated ($|J| = 380$ G) peak–peak linewidths in the a^*b, bc, and a^*c crystallographic planes is shown in Figure 3. In view of the approximations in the model there is reasonable agreement between the calculated and experimental data.

The value of J estimated for $[VO(mquin)_2]$ is considerably greater than the corresponding values of -200 G (ferromagnetic) at 300 K reported for both *N,N,N',N'*-tetramethylethylenediaminedium aquabis(malonato)oxovanadate(IV) dihydrate,[33] $[H_2tmen][VO(mal)_2(H_2O)]\cdot 2H_2O$, and *cis*-oxobis(1-phenylbutane-1,3-dionato)vanadium(IV),[34] *cis*-$[VO(pbd)_2]$, and 130 G (antiferromagnetic) for dichloro-oxobis(*N,N,N',N'*-tetramethylurea)vanadium(IV),[35] $[VOCl_2(tmu)_2]$. The larger value of $|J|$ does not correlate directly with the vanadium–vanadium separations in $[VO(mquin)_2]$ since the closest such separation (7.601 Å) is longer than the closest contacts in $[H_2tmen][VO(mal)_2(H_2O)]\cdot 2H_2O$ (6.342 Å), in *cis*-$[VO(pbd)_2]$ (5.7 Å), and in $[VOCl_2(tmu)_2]$ (7.285 Å). Although there may be a contribution to the electronic exchange *via* direct interaction, it seems highly probable that a significant pathway for this exchange is also provided by the partial overlapping of the aromatic rings of the ligands. The distance between the least-squares best planes of these rings from molecules related by a centre of inversion is 3.60 Å. This is similar to the situation in *cis*-$[VO(pbd)_2]$, with a separation between the aromatic rings of approximately 4.0 Å, where a similar pathway has been proposed for the electronic exchange interaction.[34]

Appendix

$$g_{zz} = 2.0023 - \frac{8\alpha^2\beta^2\xi C_1^2}{\Delta_2} - \frac{8\alpha^2\varepsilon^2\xi C_2^2}{\Delta_5} \quad (A1)$$

$$g_{xx} = 2.0023 - \frac{2\alpha^2\gamma^2\xi C_3^2}{\Delta_3} - \frac{2\alpha^2\delta^2\xi C_4^2}{\Delta_4} \quad (A2)$$

$$g_{yy} = 2.0023 - \frac{2\alpha^2\gamma^2\xi C_5^2}{\Delta_3} - \frac{2\alpha^2\gamma^2\xi C_6^2}{\Delta_4} \quad (A3)$$

$$g_{xy} = g_{yx} = -\frac{2\alpha^2\gamma^2\xi C_3C_5}{\Delta_3} - \frac{2\alpha^2\delta^2\xi C_4C_6}{\Delta_4} \quad (A4)$$

$$A_{zz} = P\left[-\alpha^2K + (g_{zz} - 2.0023) - \frac{2\alpha^2}{7}(4a_1^2 + 4b_1^2 - 2) + 2\frac{\xi}{7}\left(\frac{\alpha^2\gamma^2C_5C_7}{\Delta_3} + \frac{\alpha^2\delta^2C_6C_8}{\Delta_4} - \frac{\alpha^2\gamma^2C_3C_9}{\Delta_3} - \frac{\alpha^2\delta^2C_4C_{10}}{\Delta_4}\right)\right] \quad (A5)$$

$$A_{xx} = P\left[-\alpha^2K + (g_{xx} - 2.0023) - \frac{2\alpha^2}{7}(a_1^2 + b_1^2 + 3c_1^2 + 2\sqrt{3}a_1c_1 - 2) + 2\frac{\xi}{7}\left(\frac{\alpha^2\beta^2C_1C_{11}}{\Delta_2} + \frac{\alpha^2\varepsilon^2C_2C_{12}}{\Delta_5} - \frac{\alpha^2\gamma^2C_5C_7}{2\Delta_3} - \frac{\alpha^2\delta^2C_6C_8}{2\Delta_4}\right)\right] \quad (A6)$$

$$A_{yy} = P\left[-\alpha^2K + (g_{yy} - 2.0023) - \frac{2\alpha^2}{7}(a_1^2 + b_1^2 + 3c_1^2 - 2\sqrt{3}a_1c_1 - 2) - \frac{2\xi}{7}\left(\frac{\alpha^2\beta^2C_1C_{11}}{\Delta_2} + \frac{\alpha^2\varepsilon^2C_2C_{12}}{\Delta_5} - \frac{\alpha^2\gamma^2C_3C_9}{2\Delta_3} - \frac{\alpha^2\delta^2C_4C_{10}}{2\Delta_4}\right)\right] \quad (A7)$$

$$A_{xy} = P\left[-\frac{4\sqrt{3}}{7}\alpha^2c_1b_1 + g_{xy} + \frac{2\xi}{7}\left(\frac{2\alpha^2\beta^2C_1C_{13}}{\Delta_2} + \frac{2\alpha^2\varepsilon^2C_2C_{14}}{\Delta_5} - \frac{\alpha^2\gamma^2C_5C_9}{2\Delta_3} - \frac{\alpha^2\delta^2C_6C_{10}}{2\Delta_3}\right)\right] \quad (A8)$$

$$A_{yx} = P\left[-\frac{4\sqrt{3}}{7}\alpha^2c_1b_1 + g_{yx} - \frac{2\xi}{7}\left(\frac{2\alpha^2\beta^2C_1C_{15}}{\Delta_2} + \frac{2\alpha^2\varepsilon^2C_2C_{16}}{\Delta_5} - \frac{\alpha^2\gamma^2C_3C_7}{2\Delta_3} - \frac{\alpha^2\delta^2C_4C_8}{2\Delta_4}\right)\right] \quad (A9)$$

where $C_1 = a_2b_1 - b_2a_1$, $C_2 = a_5b_1 - b_5a_1$, $C_3 = -e_3b_1 + f_3a_1 + \sqrt{3}f_3c_1$, $C_4 = -e_4b_1 + f_4a_1 + \sqrt{3}f_4c_1$, $C_5 = f_3b_1 + e_3a_1 - \sqrt{3}e_3c_1$, $C_6 = f_4b_1 + e_4a_1 - \sqrt{3}e_4c_1$, $C_7 = 3e_3a_1 - 3f_3b_1 - \sqrt{3}e_3c_1$, $C_8 = -3e_4a_1 - 3f_4b_1 - \sqrt{3}e_4c_1$, $C_9 = 3f_3a_1 - 3e_3b_1 - \sqrt{3}f_3e_1$, $C_{10} = 3f_4a_1 - 3e_4b_1 - \sqrt{3}f_4c_1$, $C_{11} = 2\sqrt{3}c_2b_1 + 2\sqrt{3}b_2c_1$, $C_{12} = 2\sqrt{3}c_5b_1 + 2\sqrt{3}b_5c_1$, $C_{13} = a_2a_1 + b_2b_1 + 3c_2c_1 - \sqrt{3}(c_2a_1 + c_1a_2)$, $C_{14} = a_5a_1 + b_5b_1 + 3c_5c_1 - \sqrt{3}(c_5a_1 + c_1a_5)$, $C_{15} = a_2a_1 + b_2b_1 + 3c_2c_1 + \sqrt{3}(c_2a_1 + c_1a_2)$, $C_{16} = a_5a_1 + b_5b_1 + 3c_5c_1 + \sqrt{3}(c_5a_1 + c_1a_5)$, Δ_i = energy separation between ψ_1 and ψ_i, and K = isotropic Fermi contact contribution.

Normalisation equations:

$$\left.\begin{aligned} a_1^2 + b_1^2 + c_1^2 - 1 &= 0 \\ a_2^2 + b_2^2 + c_2^2 - 1 &= 0 \\ a_5^2 + b_5^2 + c_5^2 - 1 &= 0 \\ e_3^2 + f_3^2 - 1 &= 0 \\ e_4^2 + f_4^2 - 1 &= 0 \end{aligned}\right\} \quad \text{(A10)}$$

$$\left.\begin{aligned} a_1^2 + a_2^2 + a_5^2 - 1 &= 0 \\ b_1^2 + b_2^2 + b_5^2 - 1 &= 0 \\ c_1^2 + c_2^2 + c_5^2 - 1 &= 0 \\ e_3^2 + e_4^2 - 1 &= 0 \\ f_3^2 + f_4^2 - 1 &= 0 \end{aligned}\right\} \quad \text{(A11)}$$

Orthogonalisation equations:

$$\left.\begin{aligned} a_1a_2 + b_1b_2 + c_1c_2 &= 0 \\ a_1a_5 + b_1b_5 + c_1c_5 &= 0 \\ a_2a_5 + b_2b_5 + c_2c_5 &= 0 \\ e_3e_4 + f_3f_4 &= 0 \end{aligned}\right\} \quad \text{(A12)}$$

Acknowledgements

We thank the S.E.R.C. for financial support. Computations were performed at the University of Manchester Regional Computer Centre.

References

1 A. Abragam and B. Bleaney, 'Electron Paramagnetic Resonance of Transition Ions,' Clarendon Press, Oxford, 1970, ch. 9.
2 C. J. Gorter and J. H. Van Vleck, *Phys. Rev.*, 1947, **72**, 1128.
3 J. H. Van Vleck, *Phys. Rev.*, 1948, **74**, 1168.
4 P. W. Anderson and P. R. Weiss, *Rev. Mod. Phys.*, 1953, **25**, 269.
5 Z. G. Soos, R. T. McGregor, T. T. P. Cheung, and A. J. Silverstein, *Phys. Rev. B*, 1977, **16**, 3036.
6 D. M. S. Bagguley and J. H. E. Griffiths, *Proc. R. Soc. London, Ser. A*, 1950, **201**, 366.
7 M. Shiro and Q. Fernando, *Anal. Chem.*, 1971, **43**, 1222.
8 C. D. Garner, P. Lambert, F. E. Mabbs, and J. K. Porter, *J. Chem. Soc., Dalton Trans.*, 1972, 30.
9 D. Collison, B. Gahan, C. D. Garner, and F. E. Mabbs, *J. Chem. Soc., Dalton Trans.*, 1980, 667.
10 J. Selbin and L. Morpurgo, *J. Inorg. Nucl. Chem.*, 1965, **27**, 673.
11 J. E. Drake, J. Vekris, and J. S. Wood, *J. Chem. Soc. A*, 1968, 1000.
12 D. S. Schonland, *Proc. Phys. Soc. London*, 1959, **73**, 788.
13 A. Lund and T. Vanngard, *J. Chem. Phys.*, 1965, **42**, 2979.
14 D. Collison and F. E. Mabbs, *J. Chem. Soc., Dalton Trans.*, 1982, 1565.
15 B. Gahan and F. E. Mabbs, *J. Chem. Soc., Dalton Trans.*, 1983, 1713.
16 A. Abragam and B. Bleaney, 'Electron Paramagnetic Resonance of Transition Ions,' Clarendon Press, Oxford, 1970, pp. 745—751.
17 M. Gerloch and R. C. Slade, 'Ligand Field Parameters,' Cambridge University Press, 1973.
18 M. Gerloch and R. G. Woolley, *Prog. Inorg. Chem.*, 1984, **31**, 371.
19 M. Gerloch and L. R. Hanton, *Inorg. Chem.*, 1980, **19**, 1692.
20 D. A. Cruse and M. Gerloch, *J. Chem. Soc., Dalton Trans.*, 1977, 152.
21 D. A. Cruse and M. Gerloch, *J. Chem. Soc., Dalton Trans.*, 1977, 1613.
22 T. M. Dunn, *Trans. Faraday Soc.*, 1961, **57**, 1441; B. N. Figgis and J. Lewis, *Prog. Inorg. Chem.*, 1964, **6**, 37.
23 B. R. McGarvey, *J. Phys. Chem.*, 1967, **71**, 51.
24 C. D. Garner, I. Hillier, F. E. Mabbs, C. Taylor, and M. F. Guest, *J. Chem. Soc., Dalton Trans.*, 1976, 2258.
25 J. T. C. Van Kemenade, *Recl. Trav. Chim. Pays-Bas*, 1973, **92**, 1102.
26 P. F. Bramman, T. Land, J. B. Raynor, and C. J. Willis, *J. Chem. Soc., Dalton Trans.*, 1975, 45.
27 NAG Library, Regional Computer Centre, University of Manchester.
28 P. E. Gill and W. Murray, 'Numerical Methods for Constrained Minimization,' Academic Press, New York, 1974.
29 W. Murray, 'Methods for Constrained Optimisation, Optimisation in Action,' ed. L. C. W. Dixon, Academic Press, New York, 1976, ch. 12.
30 G. F. Kokoska, 'Low Dimensional Cooperative Phenomena,' ed. H. J. Keller, Plenum, New York, 1975, p. 171; P. M. Richards, *ibid.*, p. 147.
31 K. T. McGregor and Z. G. Soos, *J. Chem. Phys.*, 1976, **64**, 2506.
32 C. P. Slichter, 'Principles of Magnetic Resonance,' Harper and Row, New York, 1963, p. 50.
33 D. Collison, B. Gahan, and F. E. Mabbs, *J. Chem. Soc., Dalton Trans.*, 1983, 1705.
34 G. D. Simpson, R. L. Belford, and R. Biagioni, *Inorg. Chem.*, 1978, **17**, 2424.
35 B. Gahan and F. E. Mabbs, *J. Chem. Soc., Dalton Trans.*, 1983, 1695.

Received 29th January 1986; *Paper* 6/203